Liquid Crystals
Publication details, including instructions for authors and subscription information:
http://www.informaworld.com/smpp/title~content=t713926090

Effect of lateral methoxy substitution on mesomorphic and structural properties of ferroelectric liquid crystals

Alexej Bubnov[a]; Miroslav Kašpar[a]; Vladimíra Novotná[a]; Věra Hamplová[a]; Milada Glogarová[a]; Nadia Kapernaum[b]; Frank Giesselmann[b]
[a] Institute of Physics, Academy of Sciences of the Czech Republic, 182 21 Prague, Czech Republic [b] Institute of Physical Chemistry, University of Stuttgart, 70569 Stuttgart, Germany

To cite this Article Bubnov, Alexej , Kašpar, Miroslav , Novotná, Vladimíra , Hamplová, Věra , Glogarová, Milada , Kapernaum, Nadia and Giesselmann, Frank(2008) 'Effect of lateral methoxy substitution on mesomorphic and structural properties of ferroelectric liquid crystals', Liquid Crystals, 35: 11, 1329 — 1337
To link to this Article: DOI: 10.1080/02678290802585525
URL: http://dx.doi.org/10.1080/02678290802585525

Liquid Crystals,
Vol. 35, No. 11, November 2008, 1329–1337

Taylor & Francis
Taylor & Francis Group

Effect of lateral methoxy substitution on mesomorphic and structural properties of ferroelectric liquid crystals

Alexej Bubnov[a]*, Miroslav Kašpar[a], Vladimíra Novotná[a], Věra Hamplová[a], Milada Glogarová[a], Nadia Kapernaum[b] and Frank Giesselmann[b]

[a]*Institute of Physics, Academy of Sciences of the Czech Republic, Na Slovance 2, 182 21 Prague, Czech Republic;* [b]*Institute of Physical Chemistry, University of Stuttgart, Pfaffenwaldring 55, 70569 Stuttgart, Germany*

(Received 20 March 2008; final form 28 October 2008)

A new series of materials with a chiral fragment derived from lactic acid and a methoxy group as lateral substituent in different positions of the molecular core was synthesised and investigated. Derivatives with ester or ether linkages of the non-chiral chain were also studied. Depending on the molecular structure, cholesteric, twist grain boundary smectic A (TGBA*), chiral smectic A (SmA*) or chiral smectic C (SmC*) phases were detected. In derivatives with the ester linkage and a methoxy group at the nearest and the next nearest phenyl ring to the non-chiral chain these phases completely disappear. On the other hand, a methoxy group on the phenyl ring close to the chiral chain provides a compound with low layer shrinkage at the SmA*–SmC* phase transition (''de Vries'' behaviour). The temperature dependence of the spontaneous polarisation, the tilt angle, the layer spacing as well as the complex permittivity were studied and the results discussed in terms of molecular structure.

Keywords: ferroelectric liquid crystal; chiral materials; methoxy substituent; layer shrinkage; X-ray diffraction; dielectric properties; spontaneous polarisation

1. Introduction

Since the discovery of the ferroelectric properties of the chiral smectic C* (SmC*) phase (*1*), a considerable number of new chiral liquid crystalline (LC) materials possessing mesophases of various structures and physical properties have been synthesised and studied during the last three decades. Nevertheless, the design of LC materials with ferroelectric ordering tailored to certain applications still remains a crucial challenge, which needs fundamental knowledge about the relevant relationships between molecular structure and mesomorphic and physical properties and their impact on the mechanisms of the phase transitions involved (*2*).

In general, the mesomorphic properties of liquid crystals are strongly affected by the type of molecular core, the structure of the chiral part as well as by the length and character of the non-chiral chain. LC materials with a molecular core composed of three separated phenyl rings (see Figure 1) are less common than those with a molecular core consisting of a biphenyl unit, in which $\mathbf{L_1}$ or $\mathbf{L_2}$ groups are missing.

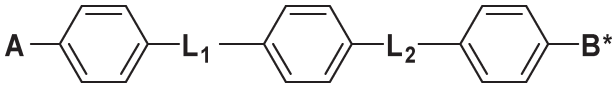

Figure 1. Schematic structure of a LC molecule with three separated phenyl rings in the core. **A** represents the alkoxy or alkoxycarbonyl chain; **B** represents a chiral part; $\mathbf{L_1}$, $\mathbf{L_2}$ can be –COO– or –OCO– groups.

A typical feature of LC materials possessing three separated phenyl rings is the lower rigidity of the core in comparison to those with the biphenyl ring. The enhanced flexibility of the molecular core typically results in rich mesomorphic behaviour.

The molecular cores of tribenzoate compounds with $\mathbf{L_1}$=$\mathbf{L_2}$=–COO– or –OCO–reported so far possessed either a methylheptyl (*3–7*) or a lactate (*3, 8–12*) chiral chain. From the latter, non-substituted compounds with an alkyllactate group as chiral part have been synthesised and studied (*8–10*, *12*). These compounds exhibit a broad temperature range of the orthogonal paraelectric chiral smectic A (SmA*) and the tilted ferroelectric SmC* phases. Recently, it has been found that some of them (*8, 9*) display rather low layer shrinkage at the SmA*–SmC* phase transition, which is a desired property in view of application demands. These compounds, identified as ''de Vries materials'' (*13*), have attracted substantial interest, but the fundamental question of the origin of their unique properties is still unsolved.

Several examples of tribenzoate compounds laterally substituted with a nitro group (*3*), a chlorine atom (*3, 10*) or one (*14–16*), two or three fluorine atoms (*17–21*) as the lateral substituents have been reported. In most cases, the lateral substitution

*Corresponding author. Email: bubnov@fzu.cz

ISSN 0267-8292 print/ISSN 1366-5855 online

DOI: 10.1080/02678290802585525
http://www.informaworld.com

lowers the phase transition temperatures in comparison to the non-substituted compounds (*3, 7, 22*).

To the best of our knowledge, no compound derived from hydroquinone ($\mathbf{L_1}$=–COO– and $\mathbf{L_2}$=–OCO–) or from terephthalic acid ($\mathbf{L_1}$=–OCO– and $\mathbf{L_2}$=–COO–) has been reported so far, as their synthesis is not accessible.

In this paper, the synthesis and characterisation are described of a new series of LC materials with a molecular core containing three benzyloxycarbonyl units with a chiral part derived from lactic acid, and with a methoxy group as attached lateral substituent at various positions on the phenyl ring in the core. The non-substituted compounds were also studied for comparison. The general chemical formula of the studied materials is presented in Table 1.

The effect of introducing the C=O group in the linkage of the non-chiral chain to the molecular core (i.e. replacement of the ester group by an ether group) was also investigated. The mesomorphic properties of the synthesised compounds were studied by polarising optical microscopy (POM), differential scanning calorimetry (DSC), X-ray diffraction, electro-optical measurements and broad-band dielectric spectroscopy.

2. Synthesis

The synthesis of the non-substituted compound (**A1**) has been described previously (*11*). The general synthetic procedure for the compounds possessing a methoxy group as the lateral substituent in different positions of the mesogenic core is presented in Scheme 1.

Octyl *p*-hydroxybenzoate (**I**, X=H, n=1) or monooctylhydroquinone (**I**, X=H, n=0) or octyl 3-methoxy-4-hydroxybenzoate (**I**, X=OCH_3, n=1) was acylated in a CH_2Cl_2/pyridine mixture for several hours with acyl chloride obtained from protected *p*-hydroxybenzoic or vanillic acid (**II**). The product (**III**) was obtained by deprotection by ammonia hydroxide (25%) in an ethanol/dichloromethane solution (1:1) at room temperature. The reaction progress was monitored by thin-layer chromatography (silica gel 60 F_{254}, Merck). When the reaction was completed the solution was poured into water and then extracted by dichloromethane. After separation the organic layer was washed by HCl, diluted in water to remove the ammonia salts, dried over sodium sulfate and then dichloromethane was evaporated. Intermediate **III** was then acylated by protected acyl chloride (**IV**) and deprotected under the same conditions as in the previous step. Crude product (**V**) was recrystallised from ethanol and reacted with 2-decyloxypropionic acid (**VI**) according to a standard esterification method yielding the final products (**A1–A5**). Preparations of 2-alkoxypropionic acids (**VI**) have been described in previous work (*22*). All final products were purified by column chromatography on silica gel (Kieselgel 60, Merck) using a dichloromethane and acetone mixture (99.5:0.5) as eluent and then crystallised twice from methanol. Structures of the intermediate and final products were confirmed by ^{1}H NMR spectroscopy using a 300 MHz Varian spectrometer and solutions in $CDCl_3$ with tetramethylsilane as an internal standard. The chemical purity of the compounds was checked by high performance liquid chromatography (HPLC), which was carried out with an Ecom HPLC chromatograph using a silica gel column (Separon 7 μm, 3 × 150, Tessek) with a mixture of 99.9% of toluene and 0.1% of methanol as eluent, and a UV–visible detector (λ=290 nm) for detection of the eluted products. For all synthesised compounds the chiral centres are in S-configuration. The chemical purity of all synthesised compounds is between 99.5 and 99.9%.

For compound **A1**, ^{1}H NMR ($CDCl_3$, 300 MHz): δ 8.28 (dd, 4H, ortho to –COOAr), 8.14 (d, 2H, ortho to –$COOCH_2$), 7.40 and 7.32 and 7.29 (d+d+d, 6H, ortho to –OCO), 4.33 (t, 2H, CH_2OCOAr); 4.22 (q, 1H, CH*), 3.25 (m, 2H, CH_2OC*), 3.58 (m, 2H, CH_2OC*), 1.60 (d, 3H, CH_3C*), 1.20–1.80 (m, 15H, CH_2, CH), 0.95 (m, 9H, CH_3).

Table 1. General chemical formula of the materials studied (X, Y, Z are the positions of the lateral positions of the methoxy group, n is the number of the C=O groups: n=0 stands for the ester group and n=1 for the ether group).

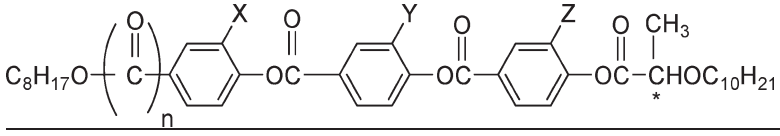

	n	X	Y	Z
A1	1	H	H	H
A2	1	H	H	OCH_3
A3	1	H	OCH_3	H
A4	0	H	OCH_3	H
A5	1	OCH_3	H	H

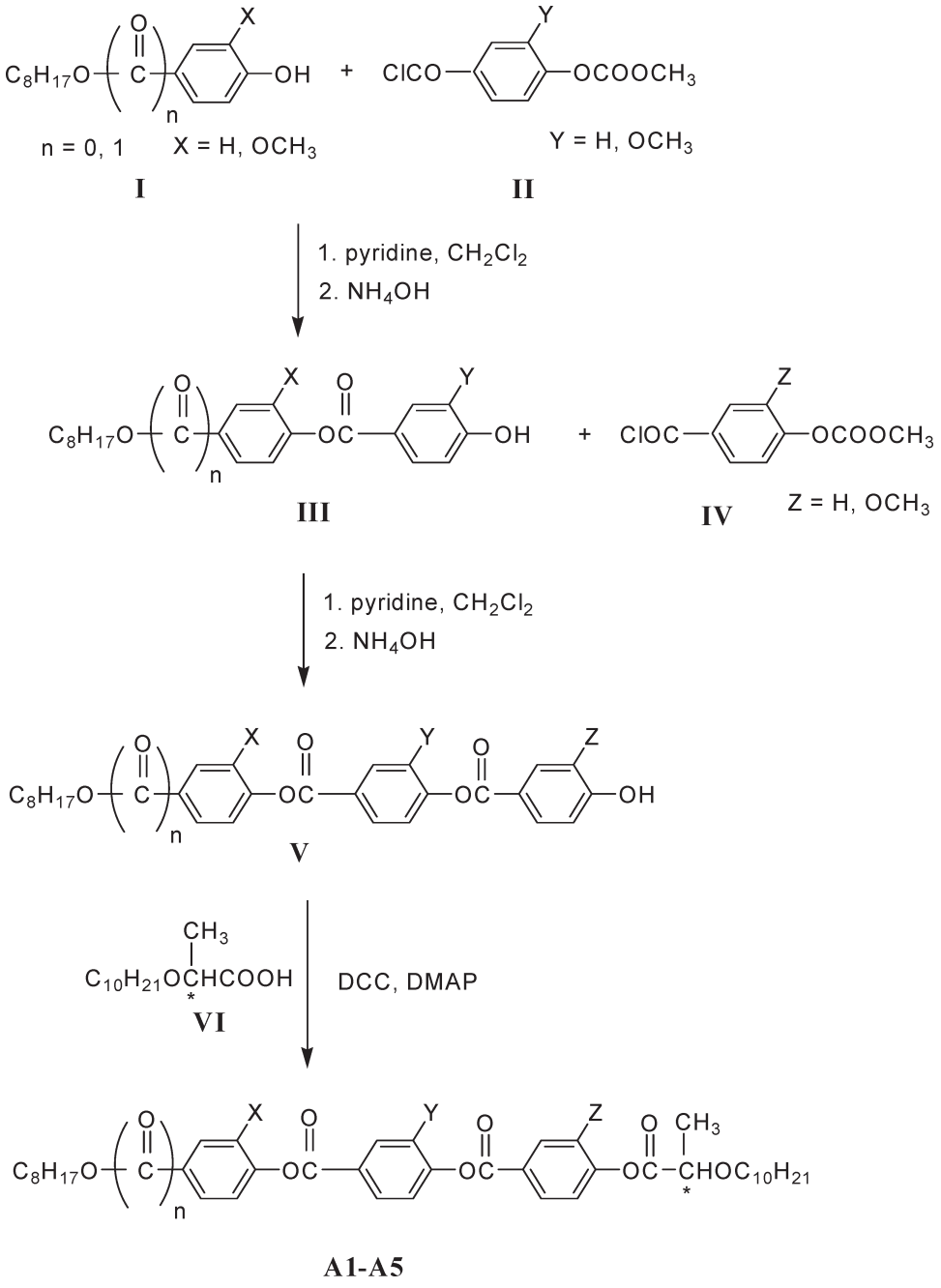

Scheme 1. General synthetic procedure for the new **A1–A5** series homologues.

For compound **A2**, ^{1}HNMR ($CDCl_3$, 300 MHz): δ 8.28 (d, 2H, ortho to –COOAr), 8.14 (d, 2H, ortho to $–COOCH_2$), 7.86 (d, 1H, para to $–OCH_3$), 7.78 (s, 1H, ortho to $–OCH_3$), 7.35–7.40 (m, 4H, ortho to –OCO), 7.20 (d, 1H, meta to $–OCH_3$), 4.34 (t, 2H, CH_2OAr), 4.20 (q, 1H, CH*), 3.95 (s, 3H, CH_3OAr), 3.58 and 3.28 (m, 2H, C*-CH_2), 1.60 (d, 3H, CH_3C*), 1.20–1.80 (m, 15H, CH_2, CH), 0.95 (m, 9H, CH_3).

For compound **A3**, ^{1}H NMR ($CDCl_3$, 300 MHz): δ 8.28 (d, 2H, ortho to –COOAr), 8.13 (d, 2H, ortho to $–COOCH_2$), 7.86 (d, 1H, para to $–OCH_3$), 7.78 (s, 1H, ortho to $–OCH_3$), 7.35 (d, 2H, ortho to –OCOCH*), 7.33 (d, 2H, ortho to –OCOAr), 7.21 (d, 1H, meta to $–OCH_3$), 4.34 (t, 2H, CH_2COOAr), 4.22 (q, 1H, CH*), 3.92 (s, 3H, CH_3OAr), 3.60 and 3.29 (m, 2H, C*-CH_2); 1.60 (d, 3H, CH_3C*), 1.20–1.60 (m, 15H, CH_2,CH), 0.95 (m, 9H, CH_3).

For compound **A4**, ^{1}H NMR ($CDCl_3$, 300 MHz): δ 8.28 (d, 2H, ortho to –COOAr), 7.86 (d, 1H, para to $–OCH_3$), 7.78 (s, 1H, ortho to $–OCH_3$), 7.35 (d, 2H, ortho to –OCOCH*), 7.20 (d, 1H, meta to $–OCH_3$), 7.10 (d, 2H, hydroquinone ortho to –OCO), 6.92 (d,

2H, hydroquinone ortho to –OR), 4.20 (q, 1H, CH*), 3.97 (d, 2H, CH_2OAr), 3.95 (s, 3H, CH_3OAr), 3.59 and 3.28 (m, 2H, C*-CH_2), 1.60 (d, 3H, CH_3C*), 1.20–1.60 (m, 15H, CH_2, CH), 0.95 (m, 9H, CH_3).

For compound **A5**, ^{1}H NMR ($CDCl_3$, 300 MHz): δ 8.25–8.30 (dd, 4H, ortho to –COOAr), 7,90 (d, 1H, para to –OCH_3), 7.80 (s, 1H, ortho to –OCH_3), 7.36 (m, 4H, ortho to –OCO), 7.30 (d, 1H, meta to –OCH_3), 4.30 (t, 2H, CH_2COOAr), 4.20 (q, 1H, CH*), 3.92 (s, 3H, CH_3OAr), 3.58 and 3.28 (m 2H, C*CH_2), 1.60 (d, 3H, CH_3C*), 1.20–1.60 (m, 15H, CH_2, CH), 0.95 (m, 9H, CH_3).

3. Experimental results

Texture observations with a polarising optical microscope, measurements of the spontaneous polarisation, the tilt angle and the dielectric constant were carried out on planar samples, where the liquid crystal sample was filled into 12 μm thick glass cells in the isotropic phase by means of capillary action. The inner surfaces of the glass plates were covered with ITO electrodes and polyimide layers unidirectionally rubbed, to achieve oriented planar anchoring. Further improvement of the alignment was achieved by application of an electric field (10–20 Hz, 40 kV cm^{-1}) applied for 5–30 min. A Linkam LTS E350 heating stage with a TMS 93 temperature programmer was used for temperature control, which enabled temperature stabilisation within ±0.1 K.

Phase transition temperatures and the enthalpies were determined by DSC (Pyris Diamond Perkin-Elmer 7) using 3–6 mg samples, which were hermetically sealed in aluminium pans. The samples were measured with cooling/heating rates of 5 K min^{-1}.

Values of the spontaneous polarisation, P_s, were evaluated from the *P(E)* hysteresis loops, which were measured during P_s reversal in an a.c. electric field, E, with a frequency of 60 Hz. The values of the tilt angle, θ_s, were determined optically from the angle difference in extinction angle between crossed polarisers under opposite d.c. electric fields of ±40 kV cm^{-1} on well-aligned samples.

The smectic layer thickness, d, was determined using Bragg's law, $n\lambda = 2d\sin\theta$, were d is calculated from the diffraction angle, θ, of the (001) smectic layer peak in the small-angle regime. Small-angle X-ray scattering (SAXS) studies were performed with Ni-filtered Cu K_α radiation (wavelength $\lambda = 1.5418$ Å), a Kratky compact camera (A. Paar) equipped with a temperature controller (temperature accuracy ~0.1 K) and a one-dimensional electronic detector (M. Braun). For SAXS studies, non-aligned samples (filled into Mark capillary tubes of 0.7 mm diameter) were used.

The frequency dispersion of the complex permittivity ($\varepsilon^* = \varepsilon' - i\varepsilon''$) was measured within the temperature range of the SmA* and SmC* phases on cooling, using a Schlumberger 1260 impedance analyser in the frequency range 1 Hz–1 MHz keeping the temperature stable during the frequency sweep within ±0.1 K. The measurements were performed under d.c. bias voltage of 0 V or 10 V. The frequency dispersion data were analysed using the generalised Cole–Cole formula for the frequency-dependent complex permittivity extended by the second term to eliminate the low-frequency contribution:

$$\varepsilon^* - \varepsilon_\infty = \frac{\Delta\varepsilon}{1 + (if/f_r)^{(1-\alpha)}} - i\frac{\sigma}{2\pi\varepsilon_0 f^n}, \qquad (1)$$

where f_r is the relaxation frequency, Δε is the dielectric strength, α is the Cole–Cole distribution parameter, ε_0 is the permittivity of a vacuum, ε_∞ is the high-frequency permittivity, σ is the d.c. conductivity and n is a fitting parameter. The measured real, $\varepsilon'(f)$, and imaginary, $\varepsilon''(f)$, parts of the dielectric permittivity were fitted simultaneously using the software "Scientist" from MicroMaths Scientist Software Corporation.

Mesomorphic properties

The phase sequences of the materials were determined from characteristic textures and their changes observed under a polarising optical microscope. Phase transition temperatures and enthalpies were measured using DSC. Mesomorphic properties of the studied compounds (**A1–A5**) are summarised in Table 2 and described below separately for the compounds with ester linkage of the non-chiral chain

Table 2. Sequence of phases, phase transition temperatures (°C), transition enthalpies (ΔH, in J g^{-1}) (measured on cooling using DSC at 5 K min^{-1}) and melting points (m.p., in °C) (measured on heating) for all the studied compounds. (• the phase exists; – the phase does not exist).

	m.p.	Cr		SmX		SmC*		TGBA*		SmA*		I
A1	92 (82.2)	•	68 (−37.9)	—		•	101 (−0.6)	—		•	105 (−5.7)	•
A2	62 (57.6)	•	8 (−40.2)	—		•	44 (−0.2)	—		•	62 (−4.7)	•
A3	73 (79.0)	•	41 (−70.8)	—		—		—		—		•
A4	77 (37.2)	•	53 (−31.3)	—		•	88 (−0.3)	•	90 (−4.0)	—		•
A5	66 (48.6)	•	38 (−31.0)	•	48 (−0.9)	—		—		—		•

to the molecular core (**A1, A2, A3, A5**) or with ether linkage (**A4**).

The non-substituted compound with an ester linkage (**A1**) exhibits a narrow paraelectric SmA* phase and a ferroelectric SmC* phase. Introduction of a methoxy group at the phenyl ring close to the chiral centre (**A2**) substantially decreases all phase transition temperatures as well as the melting point. The mesophase sequence, however, remains the same as for the non-substituted compound. The SmA* phase is broadened to a width of 40 K, which is five times broader than in **A1**. However, the SmA* and the SmC* phases in **A2** are completely monotropic. The methoxy group at the central phenyl ring (**A3**) completely destroys the mesomorphic behaviour; no LC phases are observed. Compound **A5**, with a lateral methoxy group far from the chiral centre, exhibits only a monotropic, low-temperature, non-tilted smectic phase denoted as a SmX phase.

Compound **A4** with an ether linkage of the non-chiral chain and a methoxy group at the central phenyl ring exhibits a twist grain boundary smectic A (TGBA*) phase with a narrow temperature range of about 2 K and a ferroelectric SmC* phase. Textures of the ferroelectric SmC* phase (for **A1, A2, A4**) exhibit disclination lines, which can exist in planar samples due to the strong polar anchoring at the surface. However, the distance between the disclination lines was high and irregular within the whole mesophase temperature range, indicating that the helical structure is partly unwound due to the surface anchoring. The characteristic textures of the TGBA* phase for **A4** have been observed in planar samples as well as in free-standing films (FSF) (*23*). Microphotographs of typical filament and planar fingerprint textures observed in the FSF (*23*) are presented in Figures 2(a) and 2(b), respectively.

Spontaneous polarisation and tilt angle

For compounds exhibiting a SmC* phase, the temperature dependences of the tilt angle measured optically, θ_s, and of the spontaneous polarisation, P_s, are shown in Figures 3(a) and 3(b), respectively. The measured values for θ_s consist of the spontaneous tilt angle (without electric field) and the field-induced tilt angle (due to the electroclinic effect). In principle, the field-induced tilt angle only needs to be considerd close to the phase transition. The increase of P_s at the SmA*–SmC* phase transition of **A1, A2** and **A4** is non-continuous. **A4** exhibits the highest jump at the TGBA*–SmC* phase transition, whereas the step observed for **A1** is still larger than for **A2**.

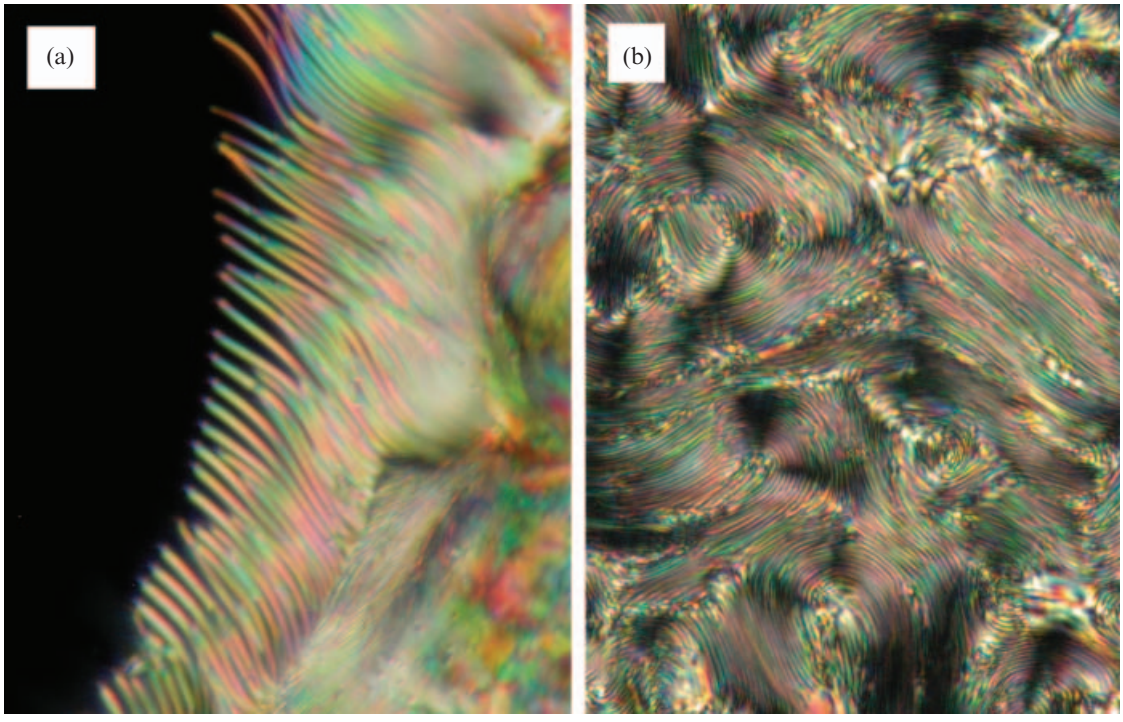

Figure 2. Microphotographs of the TGBA* phase textures of **A4** obtained on cooling: (a) filament texture at the isotropic–TGBA* phase transition in a free standing film at about 90°C and (b) fingerprint texture of the TGBA* phase obtained on a planar 12 µm thick cell at 89°C. The width of the photos is about 350 µm.

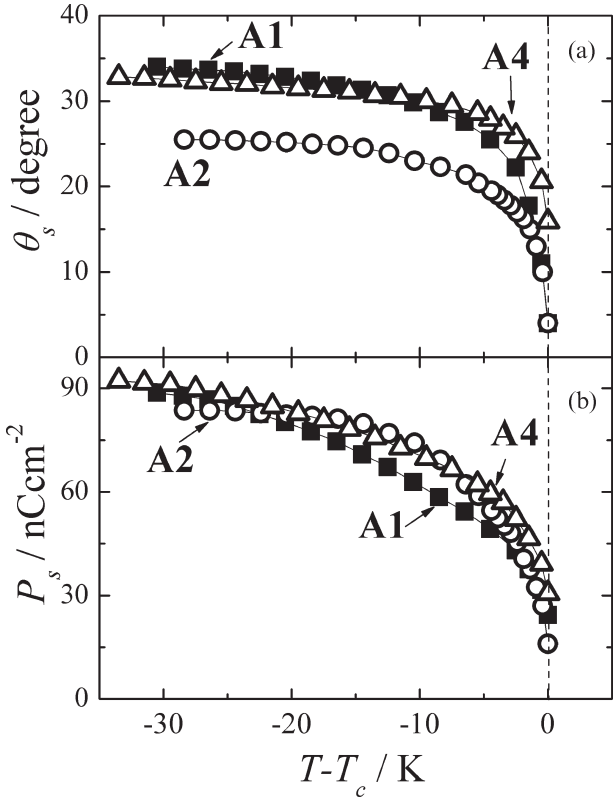

Figure 3. Temperature dependence of (a) the tilt angle, θ_s, measured optically and (b) the spontaneous polarization, P_s, for indicated compounds (**A1** squares, **A2** circles, **A4** triangles). The dashed line stands for the temperature of the phase transition to the SmC* phase.

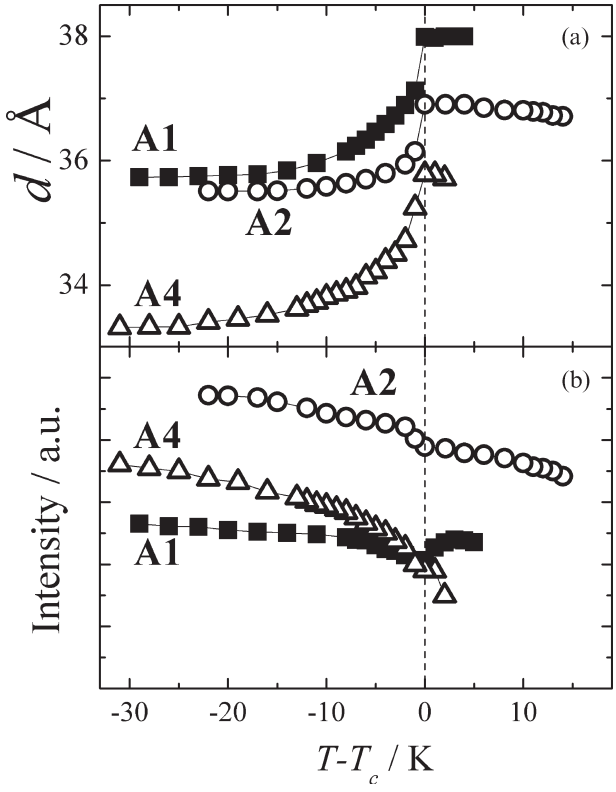

Figure 4. Temperature dependence of the (a) layer spacing, d, determined from SAXS measurements and (b) SAXS intensity of the peak maximum for the indicated compounds (**A1** squares, **A2** circles, **A4** triangles). The dashed line stands for the temperature of the phase transition to the SmC* phase on cooling.

This discontinuity might be related to a weak first-order phase transition. The temperature dependences of θ_s exhibit qualitatively similar results. Values of P_s reach 80–90 nC cm^{-2} at saturation independent of the presence of a methoxy, ester or ether linkage group, whereas the saturated values of θ_s differ significantly for different compounds (see Figure 3).

X-ray diffraction study

The results of SAXS measurements, i.e. temperature-dependent smectic layer spacings, $d(T)$, are shown in Figure 4(a). All studied compounds exhibit a slight increase of $d(T)$ in the SmA* phase on approaching the phase transition to the SmC* phase. On cooling into the tilted SmC* phase $d(T)$ clearly decreases. The decreasing layer spacing arises from the tilting of the molecules. For **A2** this decrease corresponds to layer shrinkage less than 3.5%. Such a low shrinkage comes close to a ''de Vries''-type behaviour (*13*). For **A4**, which exhibits the TGBA* phase instead of the SmA* phase, the layer shrinkage is comparable to that of **A1**.

The temperature dependence of the scattered X-ray intensities is shown in Figure 4(b). For **A1** with strong layer shrinkage, there is a pronounced drop of the intensity at the SmA*–SmC* phase transition followed by a continuous increase below the phase transition temperature. However, for **A2**, the compound with the lowest layer shrinkage, no minimum in the SAXS intensity is observed at the SmA*–SmC* transition [see Figure 4(b)]. This effect requires a more detailed study, which is in progress now and will be presented elsewhere.

The MOPAC/AM1 model was used to calculate the length of **A1** and **A2** molecules in the energy-optimised conformation. The molecular structures with the principal axis of minimum moment of inertia (''long molecular axis'') are presented in Figure 5. Taking into account the most extended conformer, the length of molecule, L, is about 42 Å for both **A1** and **A2**. The layer spacing determined by SAXS in the SmA* phase [see Figure 4(a)] is about 38 Å for **A1** and 37 Å for **A2**. Thus, the calculated lengths of the molecules agree very well with the layer spacings. The differences of about 5–10% are related to non-perfect

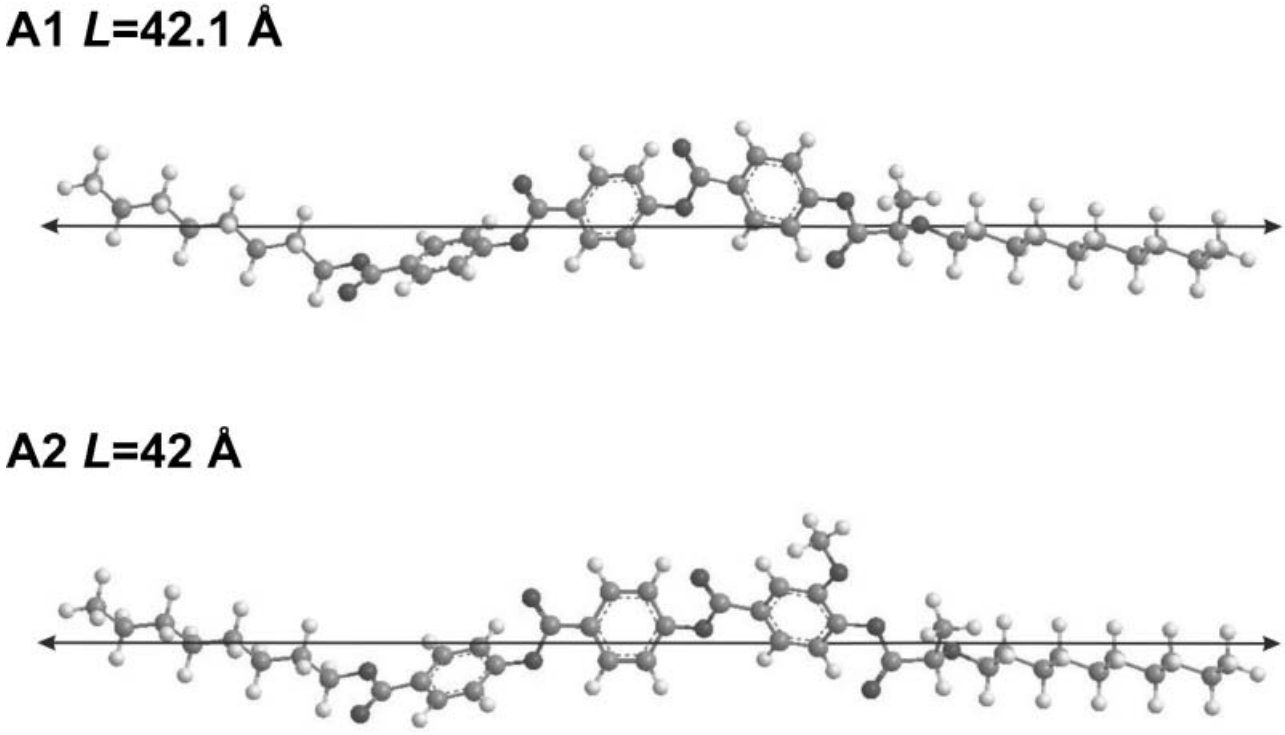

Figure 5. Conformation of the molecules (compounds **A1** and **A2** as indicated) after energy minimisation using MOPAC/AM1. L is the length of the most extended conformer.

orientational order. The orientational order parameter, S_2, can be determined according to $d \approx L/3(S_2+2)$ (*24*). With actual values for **A1** of $d=38$ Å and $L=42$ Å we obtain $S_2=0.71$, which is a quite typical value of S_2 in fluid smectics. Comparison of the models of the non-substituted **A1** with the methoxy-substituted **A2** molecules shows that the lateral substitution close to the chiral centre has only minor impact on the molecular shape.

Assuming that the length of the molecules remains unchanged at the SmA*–SmC* phase transition, the tilt of the molecules θ_{saxs} can be calculated from the temperature dependence of the layer spacing according to $d_C=d_A*\cos\theta_{saxs}$. In Figure 6 the temperature dependence of the tilt angles θ_{saxs} is shown. By comparing θ_{saxs} with the optically determined tilt angle θ_s [see Figure 3(a)] it can be seen that the values of the two tilt angles differ significantly. This well-known phenomenon (*25, 26*) is related to the fact that the two methods probe different parts of the molecular structure (see inset in Figure 6). The optical method determines the averaged orientation of the molecular core, which mainly defines the optical axis, whereas the SAXS method probes the whole molecule, by comparing the layer spacing of the SmA* phase with the d values of the SmC* phase. The inset in Figure 6 qualitatively explains the relation $\theta_{saxs}<\theta_s$.

Dielectric properties

For **A2**, dielectric absorption spectra, $\varepsilon''(f, T)$, measured in a 12 μm thick cell without d.c. bias field are presented in Figure 7. Around the SmA*–SmC* phase transition, a collective mode related to the

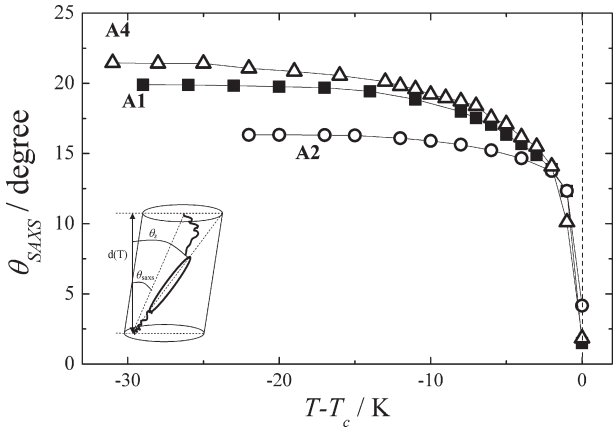

Figure 6. Temperature dependence of the tilt angle, θ_{SAXS}, calculated from the layer spacing data for the indicated compounds (**A1** squares, **A2** circles, **A4** triangles). The dashed line stands for the temperature of the phase transition to the SmC* phase. The inset shows an illustration of the molecular tilt angle θ_s measured with an electro-optical method and the tilt angle θ_{SAXS}. The tilted cylinder denotes the space occupied by an averaged molecule.

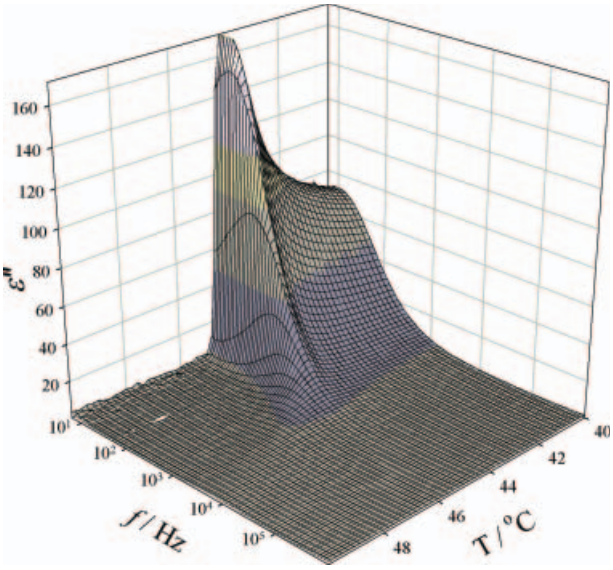

Figure 7. Dielectric absorption (ε″) spectra at zero bias electric field measured on a 12 μm thick sample cell of **A2** showing a very strong soft mode around the SmA*–SmC* phase transition.

molecular fluctuations in the tilt magnitude, the so-called soft mode, can be detected. Another collective mode related to fluctuations in azimuthal tilt direction, known as the Goldstone mode, is found in the ferroelectric SmC* phase only. The dielectric spectra were also measured under d.c. bias voltage of 10 V. The measured data were fitted by the Cole–Cole formula (see Section 3) for the frequency-dependent complex permittivity.

The temperature dependence of the fitted relaxation frequency, $f(T)$, and the dielectric increment, $\Delta\varepsilon(T)$, are shown in Figure 8 for the whole temperature range of the SmA* and SmC* phases. Whereas the soft mode in the SmA* phase is only weakly affected by the external bias field, the Goldstone mode is completely suppressed. The elimination of the Goldstone mode reveals the soft mode even in the SmC* phase, which is normally concealed by the Goldstone mode. The soft mode presented in Figure 7 is quite strong, compared to classical materials, which is typical for ''de Vries'' materials (*8*). In Table 3 the values for Δε at the SmA*–SmC* phase transition are compared for **A1** and **A2**. Without bias voltage, both soft and Goldstone modes contribute to Δε. Under sufficiently high bias, only the soft mode is present. It can be seen that the soft mode is three times stronger for the ''de Vries'' compound **A2** than that for **A1**. The temperature dependence of f and Δε is presented in Figure 8. It is observed that the bias field slightly increases the transition temperature and simultaneously broadens the phase transition. The Curie–Weiss law, i.e. the

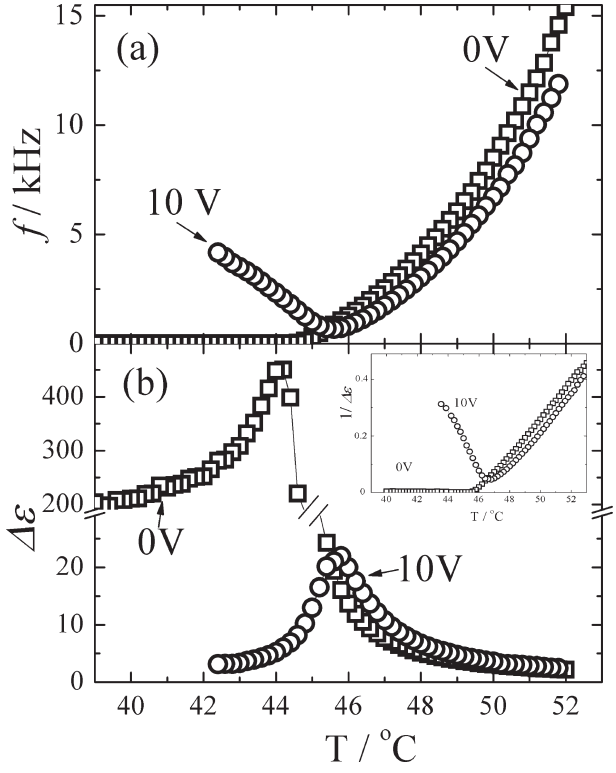

Figure 8. Temperature dependence of (a) the relaxation frequency, f, and (b) the dielectric strength, Δε, at applied bias voltage of 0 V and 10 V for **A2**. The inset shows the temperature dependence of $1/\Delta\varepsilon(T)$.

linear temperature dependence of the relaxation frequency as well as of the reciprocal permittivity, is well fulfilled for the reciprocal permittivity within about 8 K above the SmA*–SmC* transition, for the relaxation frequency only for a few K.

4. Discussion and conclusions

The effect of the lateral introduction of a methoxy group at various phenyl rings has been investigated with compounds featuring three benzyloxycarbonyl units in the molecular core and a chiral part derived from lactic acid. The introduction of the methoxy group significantly lowers melting and clearing temperatures and the temperature range of the mesophases. The compound **A2** with the methoxy group at the phenyl ring closest to the chiral chain

Table 3. Comparison of the contribution of modes to Δε at the SmA*–SmC* phase transition. Without bias both the soft and Goldstone modes contribute; under bias, Δε comes from the soft mode only.

Bias	Δε (**A1**)	Δε (**A2**)
0 V	1025	450
10 V	7.2	23.1

retains both the SmA* and SmC* phases and the transition temperature is decreased by about 40 K compared to the non-substituted variant **A1**. Introduction of the methoxy group at the central (**A3**) or at the most distant phenyl ring (**A5**) from the chiral chain eliminates the mesomorphic properties or produces only a low temperature smectic phase, respectively. A variant of compound **A3**, with the methoxy group at the central core, but with modified linkage to the non-chiral chain (**A4**, ester linkage is replaced by ether) exhibits a SmC* phase like **A1** and **A2**, but instead of a SmA* phase, a TGBA* phase appears.

The methoxy-substituted compound **A2** comes close to ''de Vries''-type behaviour. It shows a much smaller layer shrinkage at the SmA*–SmC* phase transition ($d_{SmC*}/d_{SmA*} \sim 3.5\%$) than the non-substituted **A1** ($d_{SmC*}/d_{SmA*} \sim 6.4\ \%$). The strong soft mode detected by dielectric spectroscopy [similar to that reported by Cheng *et al.* (*5*)] in the vicinity of the SmA*–SmC* phase transition in compound **A2** is in accordance with the ''de Vries'' character of this phase transition.

Acknowledgements

This work is supported by the German–Czech bilateral programme DAAD (German Academic Exchange Service)–ASCR (Academy of Science of the Czech Republic) No. D11-CZ7/06-07 & D7-CZ8/08-09 and also partially by projects No. IAA100100710 from the Grant Agency of the Academy of Sciences of the Czech Republic, No. 202/05/0431 from the Czech Science Foundation and No. AVOZ10100520. Authors (A.B. and V.N.) greatly acknowledge Dr. S. Bezner and Dr. C. Hägele for help with the SAXS measurements.

References

(1) Meyer R.; Liebert L.; Strzelecki L.; Keller P. *J. Phys. Lett., Paris* **1975**, *36*, 69–71.
(2) Lagerwall J.P.F.; Giesselmann F. *ChemPhysChem* **2006**, *7*, 20–45.
(3) Dzik E.; Mieczkowski J.; Gorecka E.; Pociecha D. *J. Mater. Chem.* **2005**, *15*, 1255–1262.
(4) Cheng Y.; Xu W.; Wang X.; Sun L.; Zhao B. *Liq. Cryst.* **2004**, *31*, 1407–1412.
(5) Cheng J.; Cheng Y.; Ruan W.; Xu W.; Zhao B.; Zhang G. *J. Chem. Phys.* **2005**, *122*, 214913.
(6) Kuczynski W.; Goc F.; Dardas D.; Dabrowski R.; Hoffmann J.; Stryla B.; Malecki J. *Ferroelectrics* **2002**, *274*, 83–100.
(7) Zywucki B.; Kuczynski W.; Malecki J. *Ferroelectrics* **2003**, *297*, 91–105.
(8) Krueger M.; Giesselmann F. *Phys. Rev. E* **2004**, *71*, 041704.
(9) Bezner S.; Krueger M.; Hamplová V.; Glogarová M.; Giesselmann F. *J. Phys. Chem.* **2007**, *126*, 054902.
(10) Kašpar M.; Hamplová V.; Pakhomov S.A.; Bubnov A.M.; Guittard F.; Sverenyák H.; Stibor I.; Vanek P.; Glogarová M. *Liq. Cryst* **1998**, *24*, 599–605.
(11) Pakhomov S.A.; Kašpar M.; Hamplová V.; Bubnov A.M.; Sverenyák H.; Glogarová M.; Stibor I. *Ferroelectrics* **1998**, *212*, 341–348.
(12) Giesselmann F.; Zugenmaier P.; Dierking I.; Lagerwall S.T.; Stebler B.; Kašpar M.; Hamplová V.; Glogarová M. *Phys. Rev. E* **1999**, *60*, 598–602.
(13) de Vries A. *Mol. Cryst. Liq. Cryst. Lett.* **1977**, *41*, 27–31.
(14) Essid S.; Manai M.; Gharbi A.; Marcerou J.P.; Rouillon J.C. *Liq. Cryst.* **2005**, *32*, 307–313.
(15) Huang C.C.; Liu Z.Q.; Cady A.; Pindak R.; Caliebe W.; Barois P.; Nguyen H.T.; Ema K.; Takekoshi K.; Yao H. *Liq. Cryst.* **2004**, *31*, 127–135.
(16) Essid S.; Manai M.; Gharbi A.; Marcerou J.P.; Rouillon J.C.; Nguyen H.T. *Liq. Cryst.* **2004**, *31*, 1185–1193.
(17) Cruz C.D.; Rouillon J.C.; Marcerou J.P.; Isaert N.; Nguyen H.T. *Liq. Cryst.* **2001**, *28*, 125–137.
(18) Cruz C.D.; Rouillon J.C.; Marcerou J.P.; Isaert N.; Nguyen H.T. *Liq. Cryst.* **2001**, *28*, 1185–1192.
(19) Cruz C.D.; Grelet E.; Rouillon J.C.; Marcerou J.P.; Sigaud G.; Pansu B.; Nguyen H.T. *Liq. Cryst.* **2001**, *28*, 1415–1423.
(20) Douali R.; Legrand C.; Laux V.; Isaert N.; Joly G.; Nguyen H.T. *Phys. Rev. E* **2004**, *69*, 031709.
(21) Shubashree S.; Sadashiva B.K.; Dhara S. *Mol. Cryst. Liq. Cryst.* **2002**, *381*, 21–32.
(22) Kašpar M.; Hamplová V.; Pakhomov S.A.; Stibor I.; Sverenyák H.; Bubnov A.M.; Glogarová M.; Vanek P. *Liq. Cryst.* **1997**, *22*, 557–561.
(23) Dierking I. *Textures of Liquid Crystals*; Wiley-VCH Verlag: Weinheim, 2003.
(24) Lagerwall J.P.F.; Giesselmann F.; Radcliffe M.D. *Phys. Rev. E* **2002**, *66*, 031703.
(25) Goodby J.W.; Stanley A.J.; Both C.J.; Nishiyama I.; Vuijk L.D.; Styring P.; Toyne K.J. *Mol. Cryst. Liq. Gryst.* **1994**, *243*, 231–298.
(26) Piecek W.; Raszewski Z.; Perkowski P.; Przedmojski J.; Kedzierski J.; Drzewinski W.; Dabrowski R.; Zielinski J. *Ferroelectrics* **2004**, *310*, 125–129.